„Incorporation of mRNA in lamellar lipid matrices for parenteral administration“

Antje Ziller[1]; Sara S. Nogueira[1,2]; Eva Hühn[1]; Sergio S. Funari[3]; Gerald Brezesinski[4]; Hermann Hartmann[5]; Ugur Sahin[2]; Heinrich Haas[2]; Peter Langguth[1*]

[1]Department of Pharmaceutics and Biopharmaceutics, Johannes Gutenberg University Mainz, 55099 Mainz, FRG

[2]BioNTech RNA Pharmaceuticals, 55131, Mainz, FRG

[3]HASYLAB, 22607 Hamburg, FRG

[4]Max Planck Institute of Colloids and Interfaces, 14476 Potsdam, FRG

[5]Institute for Molecular Biophysics, Johannes Gutenberg University Mainz, 55099 Mainz, FRG

*to whom correspondence should be addressed at:

Institute of Pharmacy and Biochemistry
Johannes Gutenberg University Mainz
D-55099 Mainz, FRG

Tel: ++49-6131-3925746

e-mail: langguth@uni-mainz.de

ABSTRACT

Insertion of high molecular weight messenger RNA (mRNA) into lyotropic lipid phases as model systems for controlled release formulations for the mRNA was investigated. Low fractions of 1,2-dioleoyl-3-trimethylammonium-propane (DOTAP) were used as an anchor to load the mRNA into a lamellar lipid matrix. Dispersions of zwitterionic lipid in the aqueous phase in the presence of increasing fractions of mRNA and cationic lipid were prepared, and the molecular organization was investigated as a function of mRNA and cationic lipid fraction. Insertion of both, cationic lipid and mRNA was clearly proven from the physicochemical characteristics. The d-spacing of the lipid bilayers, as determined by small angle x-ray scattering (SAXS) measurements, responded sensitively to the amount of inserted DOTAP and mRNA. A concise model of the insertion of the mRNA in the lipid matrices was derived, indicating that the mRNA was accommodated in the aqueous slab between lipid bilayers. Depending on the DOTAP and mRNA fraction, a different excess of water was present in this slab. Results from further physicochemical characterization, including determination of free and bound mRNA, zeta potential and calorimetry data, were in line with this assumption. The structure of these concentrated lipid/mRNA preparations was maintained upon dilution. The functionality of the inserted mRNA was proven by cell culture experiments using C2C12 murine myoblast cells with the luciferase-encoding mRNA. The described lipid phases as carriers for the mRNA may be applicable for different routes of local administration, where control of the release kinetics and the form of the released mRNA (bound or free) is required.

Keywords: Lipoplexes, liposomes, lipid bilayers, RNA, drug delivery, gene delivery, SAXS, X-rays, cationic lipid, nanoparticles, precision medicine

INTRODUCTION

Nanomedicines composed of mRNA and carrier molecules are gaining increasing interest for a wide spectrum of therapeutic applications, including tumor therapy, vaccination or protein replacement therapy [1–4]. Several new pharmaceutical products, mostly in the field of tumor therapy, have reached the level of clinical trials [3–6]. For administration of mRNA to patients, formulations are required to minimize interactions of the mRNA with the biological environment (e.g. serum), protect the mRNA from degradation by RNases while ensuring the intended release profile, deliver the mRNA to the target site, mediate binding and uptake by the target cells and ensure efficient translation of the encoded antigen. Lipid-based carrier systems have traditionally been of paramount interest for nucleic acid delivery in their role as non-viral gene delivery vehicles [7,8]. Previous studies have dealt with DNA and siRNA cargos in lipid carrier systems [8–10], and with mRNA in terms of transfection systems [11–14]. From previous studies, mostly on DNA and partially also on siRNA based systems, insight into general aspects of their molecular organization and structure function coherencies could be obtained [15–20]. Rädler et al. have investigated the structure of DNA-cationic liposome complexes with various methods including X-ray scattering [21], in which they revealed a lamellar organization of these lipoplexes. In further studies, the phase diagram of such systems was elucidated to detail [7,22,23]. Besides the lamellar phase, many other types of molecular organization, including hexagonal and cubic phases were determined. In particular, the balance between lamellar and inverse hexagonal phases of the DNA-cationic liposome complexes was considered relevant for the transfection efficacy of such systems. So far, not so much research has been performed on the structure of lipid phases comprising mRNA. However, the general understanding of the molecular organization of nucleotide-lipid assemblies as obtained from different DNA lipoplex systems may, at least partially, also be applicable for systems comprising mRNA [24–26].

Recently, novel intravenously injectable mRNA-lipoplex formulations for application in tumor immunotherapy have been developed [3], where high molecular weight mRNA coding for tumor antigens is delivered to lymphoid organs. These mRNA lipoplex formulations comprise mixtures of cationic and zwitterionic lipids where, due to defined size, charge and further physicochemical properties, selective targeting of antigen presenting cells (APCs) is obtained. On this basis, several clinical studies have been initiated [3,5] or are in advanced stages of planning.

In the present study, we focused on lipid-based carrier systems for the mRNA, which may be useful for various further administration routes (intradermal, intratumoral, intranodal) [27], where besides protection from degradation, control of the mRNA release from the carrier is required. In previous work, we have shown that mRNA lipoplex nanoparticles formed from cationic liposomes (DOTMA/DOPE) are suitable for protection of the mRNA from serum degradation and allow accurate control of the mRNA expression profile after intravenous injection [3]. Now we formed concentrated lipidic dispersions (100 mg/ml) where we applied a large excess of a zwitterionic lipid, either egg-phosphatidylcholine (80 %, EPC) or 1,2-Dioleoyl-*sn*-glycero-3-phosphocholine (DOPC) as a matrix, into which a low fraction of cationic lipid was inserted. As a cationic lipid, the commonly used and well characterized DOTAP was chosen since it is considered to also have a lower toxicity in comparison to many other cationic lipids [28]. We investigated whether the cationic lipid could serve as an anchor to load the mRNA into the lipid matrix in order to form a system for controlled mRNA release. As zwitterionic lipid matrices, established lipid components were employed for which abundant data on the application as pharmaceutical carrier systems are available and which, in principle can be suitable for pharmaceutical development of clinical trial materials [29]. Dynamic light scattering (DLS), differential scanning calorimetry (DSC) and small angle x-ray scattering (SAXS) were applied to monitor the structure of the lipid/mRNA systems. The results concisely indicate that mRNA could be inserted into the lipid phases by using rather low molar fractions of cationic lipid as an anchor. A concise molecular model of the mRNA insertion into the lipid bilayer system was derived describing fundamental aspects of all systems in a generalized manner. Cell culture experiments demonstrated the principal functionality of the mRNA in these systems.

MATERIALS & METHODS

1. MATERIALS

mRNA was synthesized by BioNTech RNA Pharmaceuticals GmbH (Mainz, Germany) using internal protocols as published earlier [30]. EPC 80, DOPC and DOTAP were purchased from Lipoid GmbH (Ludwigshafen, Germany). Ampuwa was obtained from Fresenius Kabi Deutschland GmbH (Bad Homburg vor der Höhe, Germany) and Chloroform was purchased from Sigma-Aldrich (St. Louis, USA). For the solvent D-(+)-Trehalose [31] dihydrate from saccharomyces cerevisiae was obtained from Sigma-Aldrich (St. Louis, USA) as well. RNaseZap$^{(R)}$ was purchased from Ambion$^{(R)}$-Life Technologies (Carlsbad, USA).

2. METHODS

RNase-free working

A RNase-free environment was ensured by treating glassware at 300 °C for more than four hours while RNaseZap$^{(R)}$ (Ambion®, Thermo Scientific™, Darmstadt, Germany) was used for plastic components and all surfaces. Furthermore, RNase-free lab materials and substances were employed.

mRNA integrity

The integrity of mRNA in the formulations after preparation was tested with the commercially available RNA 6000 Nano Kit using the Agilent 2100 Bioanalyzer (Agilent, Santa Clara, USA) lab-on-chip system that is based on a capillary electrophoresis. Samples were mixed with an equal amount of formamide buffer (23.8 M formamide, 8.7 mM SDS, 18.0 mM EDTA) before testing. A 1 µl sample corresponding to a mRNA-concentration of 25-250 ng/µl was filled into the wells in an appropriate chip. Electropherograms were obtained by reaction with a fluorescent dye and translated into gel-like images (bands).

Lipoplex preparation with film method

For lipoplexes, the required amount of lipids[1] was dissolved in chloroform to obtain a homogeneous mixture of lipid. The organic solvent was removed via dry nitrogen stream (for small volumes < 1ml) or via rotary evaporation (for higher volumes > 1ml) with a Büchi® Rotavapor R-3 (BÜCHI Labortechnik GmbH, Essen, Germany). The resulting thin lipid film was dried under vacuum overnight using a CHRIST Alpha 1-4 freeze-dryer (B. Braun Melsungen AG, Melsungen, Germany) to remove all residual solvent. Thereafter, a 10 % trehalose solution containing the mRNA was added to obtain a lipid concentration of 100 mg/ml. The suspension was briefly vortexed and left overnight at room temperature for full hydration.

Table 1: Tested systems with EPC as a matrix lipid and different proportions (mol%) of DOTAP and mRNA with the resulting (+/-) charge ratios and the implemented measurements.

mRNA / DOTAP	0		5		10	
0	0	*	0	*	0	*
5	0	*	1/1	*	1/2	*
10	0	*	2/1	*	1/1	*

[1] Example calculation for 90 mol% DOPC with 10 mol% DOTAP with 100 mg/ml lipid concentration:

$$DOPC\colon 0.9mol * 786.113\frac{g}{mol} = 707.502g \wedge DOTAP\colon 0.1mol * 698.542\frac{g}{mol} = 69.854g$$

$$707.504g + 69.854g = 777.358g$$

$$DOPC\colon \frac{777.358g}{100mg} = \frac{707.502g}{x} \wedge DOTAP\colon \frac{777.358g}{100mg} = \frac{69.854g}{x}$$

$x =$91.01 mg $\qquad\qquad$ $x = 8.99mg$

Table 2: Tested systems with DOPC as a matrix lipid and different proportions (mol%) of DOTAP and mRNA with the resulting (+/-) charge ratios and the implemented measurements.

mRNA DOTAP	0		2.5		5		10		20	
0	0/0	* #	0	*	0	* #	0	*	0	* °
1	1/0	#			1/5	#				
2	2/0	#			1/2.5	#				
2.5	2.5/0	*	1/1	*	1/2	* #	1/4	*	1/8	* + x
3	3/0	#			1/1.67	#				
4	3/0	#			1/1.25	#				
5	5/0	* #	2/1	*	1/1	* #	1/2	*	1/4	* + x
6										
7.5									1/3	+ x
8										
10	10/0	* #	4/1	*	2/1	*	1/1	*	1/2	* + x °
11.4									1/1.75	+ x
13									1/1.5	+ x
15									1/1.33	+ x
16									1./1.25	+ x
17.4									1/1.12	+ x
20									1/1	+ x °
25									1.25/1	+ x
30									1.5/1	+ x °
35									1.75/1	+ x
40									2/1	+ x °
45									2.25/	+ x
50									12.5/1	+ x °

* SAXS
+ Zeta potential
x Incorporated mRNA
DSC
° Transfection
(Legend for tables 1 and 2)

Small-angle X-ray scattering (SAXS)

The structure of the lipid-mRNA-layers was investigated by small angle X-ray scattering (SAXS) measurements. For this purpose, a Kratky camera with a slit collimation system was used and the scattered intensities were recorded with a linear position sensitive detector (PSD-50M, M. Braun, Germany) in the q-range between 0.006 $Å^{-1}$ and 0.6 $Å^{-1}$ at a stable temperature of 20±2 °C. Each sample was measured three times with measurements of the solvent in between, while the background was subtracted afterwards. Slit smearing was corrected by using a modified version of the Lake algorithm and application of a Savitzky-Golay smoothing kernel to the de-smeared intensities.

For the study of the influence of the dilution on the structure and d-spacing of the formulations, measurements were conducted at the A2 beamline at HASYLAB/DESY (German Electron Synchrotron Hamburg, Germany). MarCCD165 2D detector with a sample-detector distance of 1.263m (calibration with RTT (rat tail tendon)) and a q-range between 0.002$Å^{-1}$ and 0.34$Å^{-1}$ was used for the SAXS-recording. Mark-tubes consisting of borosilicate glass (outside-Ø 2.0 mm, wall thickness 0.01 mm, length 80 mm, Müller&Müller, Schönwalde, Germany) were utilised as a container for the samples. The temperature was held constant at 25 °C. An exposure time 100 up to 400 s was chosen. Data was analysed with the A2 tool software version 0.31a. To correct the background 10 % trehalose solution as solvent was filled into the same capillary, while the scattering curve was subtracted from the sample curve.

Zeta Potential measurements

Zeta potentials were determined on a Malvern Nano ZS (Malvern Instruments Ltd, Worcestershire, United Kingdom) with the Malvern Zetasizer Software 7.11. The calculation was done automatically by using the Smoluchowski approximation. The laser has a wavelength of 633 nm. Each sample was diluted with 10 % trehalose solution to yield a lipid concentration of 0.08 mg/ml and was measured at a temperature of 25 °C. Experiments were carried out with two independent samples measured in triplicates.

Determination of free mRNA

The amount of mRNA which is encapsulated in the lipoplexes was determined by measurement of the amount of mRNA which is not bound to the lipoplexes. This was carried out with the Quant-iT™ RiboGreen® RNA Assay (Life Technologies, Thermo Fisher Scientific Inc., Karlsruhe, Germany) by diluting the samples, adding fluorescein and detecting the fluorescence intensity with TECAN infinite F200 (Tecan Group Ltd., Männedorf, Switzerland). The wavelength of excitation was 465 nm and the emission wavelength was 535 nm. Samples were measured from below and the gain was adjusted to 130. The amount of free mRNA was subtracted from the total amount of mRNA to obtain the encapsulated mRNA. In total, the samples were diluted 1:16000 for measurement (1:8 before the Ribogreen® RNA Assay, 1:2000 while performing the assay). Experiments were carried out with two independent samples measured in triplicates.

Determination of phase transition temperature (T_m)

The phase transition temperature was measured by differential scanning calorimetry (DSC) using the Mettler-Toledo DSC 1 (Mettler-Toledo GmbH, Gießen, Germany) calorimeter under a nitrogen atmosphere. 20 µl of each formulation was filled into an aluminium crucible (Mettler-Toledo, aluminium crucible standard, 40 µl, with pin and lid), hermetically sealed and measured together with

a trehalose sample as reference since all samples were measured in presence of trehalose. The samples were cooled to – 40 °C with liquid nitrogen and subsequently heated up to 20°C. The cooling rate was 2 °C/min while the heating rate was set to 1 °C/min. Reaching – 40 °C the temperature was held constant for 5 minutes. The temperature program was repeated once.

Transfection efficiency

C2C12 myoblast cells were cultured in Dulbecco's modified Eagle's medium (DMEM) supplemented with 10 % fetal bovine serum (not inactivated) at 37 ◦C under an atmosphere with 5 % CO_2. Cells were seeded onto 96-well plates at a density of 5×10^3 cells per well for luciferase and XTT assay. After 24 h, the cells were washed with phosphate-buffered saline (PBS) and the diluted lipoplexes containing 1 µg of luciferase-encoded mRNA in Opti-Mem™ medium were added to each well. After 6 h of incubation, the culture media was replaced with fresh culture medium. The culture media was removed after 24 h and washed with 0.5 ml of PBS. 0.05 ml of PBS and reporter lysis buffer were then added to each well to lyse the cells. The relative light units (RLU) were measured using a TECAN infinite P200 PRO (Tecan Group Ltd., Männedorf, Switzerland) and normalized to the viability assay (XTT). XTT assay was done with XTT Cell Proliferation Kit II (Sigma-Aldrich GmbH, St. Louis, USA). Samples were treated according to the protocol and the readout was done after 2 hours. The wavelengths for measurement were set to 450 and 630 nm. As positive control, the untreated cells were used. Viability was calculated with the following equation: Cell viability [%] = ((treated cells-blank) / (untreated cells-blank)) * 100 %. Experiments were carried out with two independent samples measured in triplicates.

RESULTS

Small angle scattering (SAXS) measurements were performed with concentrated and diluted lipid phases. For the lipid matrices, two systems, either EPC liposomes or DOPC liposomes were used. Increasing molar fractions (up to 10 mol%) of the cationic lipid DOTAP were integrated into the zwitterionic lipid matrices, and to all systems, various amounts of mRNA (up to 20 mol%) were loaded. The amount of mRNA was always calculated in mol% with respect to single nucleotides irrespective of the total number of nucleotides per mRNA. The molar mass of one repeat unit of 330 Da was taken as a basis for the calculation. With one negative charge per nucleotide, a formulation with 5 mol% of DOTAP and 5 mol% of mRNA was equivalent to a charge ratio DOTAP/mRNA of 1/1 (+/-). First feasibility experiments were performed with EPC liposomes as this lipid was a readily available and established system for liposome formation. For further experiments, DOPC was selected as matrix lipid to obtain a unique compound with defined properties for matrix formation.

Fig. 1 shows the X-ray scattering curves for a series of measurements using EPC as a lipid matrix under various conditions (see table 1 for details). Shown are (from bottom to top) the scattering curves of (i) pure EPC, (ii) EPC where mRNA was present in the aqueous phase, (iii) EPC in a mixture with 5 mol% of DOTAP, (v) EPC in a mixture with 5 mol% of DOTAP and additionally 5 mol% of mRNA and (v) EPC in a mixture with 5 mol% of DOTAP and additionally 10 mol% of mRNA. In this selection, the general features of the scattering curves can be well recognized. The pure EPC liposomes show a typical scattering curve as expected for lamellar liposomes where equidistant Bragg peaks, resulting from the lamellar organization of the bilayers, are present. The d-spacings (lamellar spacings) can be readily derived from the peak positions as:

$$d = \frac{n \cdot 2\pi}{q_{max(n)}} \qquad (1)$$

Here q is the momentum transfer, with $q=4\pi \sin\theta/\lambda$, with n the order and q_{max} the maximum position of the respective Bragg peak, λ the wavelength, and θ the angle. The d-spacing that can be derived from Bragg peaks is slightly above 70 Å. Also in the presence of mRNA, the lamellar order is maintained.

Bragg peaks at the same positions as without mRNA are still visible, although they are lower in intensity. On the contrary, if DOTAP (5 mol%) is present in the membrane, in the range of 0.1 $Å^{-1}$ no more Bragg peaks are visible, and the scattering curve is dominated by the unstructured signal resulting from the individual bilayer scattering (form factor) between 0.5 and 2.5 $Å^{-1}$. At a closer look, an easily discernible, small peak at very low q (at about 0.027 $Å^{-1}$, indicated by the arrow) can be seen, which is expected to result from the extended d-spacing due to electrostatic repulsion between positively charged DOTAP of about 230 Å.

However, when also mRNA was present in the EPC/DOTAP formulations, the lamellar organization with shorter d-spacing was recovered where even orders of Bragg peaks pointing towards lamellar peaks are observable. The peak maxima are now at slightly lower q numbers in comparison to pure EPC, indicating that the d-spacing is longer. It further increases if more mRNA (10 mol%) is added to the same system.

The observations can be explained qualitatively by the repulsive or attractive electrostatic interaction between the charged moieties in the membranes. Although EPC membranes possess zwitterionic headgroups, they carry an overall negative charge and do not interact with the negatively charged mRNA. The presence of positively charged DOTAP leads to repulsive interactions between the bilayer membranes, resulting in a dramatic increase of d-spacing between the membranes along the perpendicular axis of the membrane plane. In the presence of mRNA in the EPC/DOTAP system, the mRNA is inserted into the aqueous space between the bilayers, leading to a shielding of the electrostatic repulsion and entanglement between adjacent membranes.

To further elucidate these coherences, equivalent systems were assembled using DOPC instead of EPC as a lipid matrix. While EPC is a mixture derived from natural lipids, DOPC has the advantage of being a pure and well defined synthetic molecule, thus allowing further physicochemical analysis (e.g. by calorimetry). A wider range of DOTAP and mRNA fractions was systematically investigated such as shown in table 2. By different combinations of the DOTAP and mRNA fractions, different charge ratios (+/-), as calculated from the amounts of DOTAP and mRNA nucleotides, were obtained. The table depicts the conditions that were investigated.

The general effects of DOTAP and mRNA insertion into the DOPC lipid matrices were similar to those observed with EPC, namely (i) no effect of RNA on d-spacing, (ii) strong increase of d-spacing and loss of correlation on insertion of DOTAP, and (iii) recovery of lamellar organization if both, DOTAP and mRNA, were present where, as a trend, the d-spacing increased with increasing mRNA content indicated by a monotonous shift of the peak position towards lower q. As an example, the results with 5 mol% DOTAP and different amounts of mRNA in the DOPC membranes are shown in Fig. 2. Similar results were obtained also for experiments with 2.5 and 10 mol% of DOTAP in the DOPC (see supplementary data).

Careful analysis of the changes of d-spacing as a function of DOTAP and mRNA fraction gained further insight into the insertion characteristics of the mRNA into lipid matrices and led to a generic model of the insertion behavior. To this end, the results from the several measurements with different molar fractions of DOTAP in the lipid matrix and several amounts of mRNA were plotted together in one graph. All data plots are given as a function of the DOTAP/mRNA ratio[2], irrespective of the DOTAP/DOPC ratio. In this manner, the results from the sample with 2.5 mol% DOTAP and 5 mol% mRNA are given at the same x-axis position as those with 5 mol% DOTAP in combination with 10 mol% mRNA, and so on.

[2] The charge ratio was calculated as follows: one positive charge for the DOTAP (molar mass of 670 Da) and one negative charge of each nucleotide, with a molar mass of 330 Da were assumed.

In Fig. 3, d-spacings (top) zeta potentials (middle) and the fraction of the free mRNA (bottom) are plotted together as a function of the (+/-) DOTAP to mRNA charge ratio.

For the d-spacings (Fig. 3 top), it can be seen, that in excess of DOTAP (+/- > 1) the value changes only marginally as a function of charge ratio. Only close to charge equilibrium and below (+/- < 1), the d-spacing increases monotonously, where similar values are found for similar charge ratios. The effect on the d-spacing depended only on the DOTAP to mRNA ratio which is also the charge ratio but was independent from the DOTAP molar fraction in the DOPC matrix. In other words, systems with (2.5 mol% DOTAP / 5 mol% mRNA) and (5 mol% DOTAP / 10 mol% mRNA), which had both the same DOTAP to mRNA (+/-) ratio of 1/2 had also a very similar d-spacing, and so on.

The systems were further investigated by measurements of the free and bound mRNA, results shown in Fig. 3 (bottom). To quantify mRNA, a commercial fluorescence-based kit was used, where the dye only shows fluorescence if it is intercalated into the mRNA. Thus, the mRNA which is accessible and non-accessible to the dye can be differentiated. Here, with an excess of DOTAP (+/- > 1), no fluorescence was present, indicating that the mRNA was not accessible to the dye. With an excess of mRNA (+/- < 1), the fluorescence, and therefore the amount of accessible mRNA monotonously increased, resulting in a decrease of the fraction of non-accessible mRNA. In the graph, the fraction of free mRNA as a function of (+/-) DOTAP to mRNA ratio is shown, where the identical scaling of the x-axis as for the d-spacing was selected.

The change of slope occurred roughly at a charge ratio of 1/1, and the amount of mRNA which was taken out of the system was roughly equivalent to the amount of added DOTAP. Apparently, binding of the mRNA (nucleotides) to DOTAP occurred in a 1/1 (+/-) ratio, resulting in inhibition of the accessibility for the intercalating dye.

Accordingly, measurements of the zeta potential in the formulations showed a switch of the charge at a DOTAP to mRNA ratio of about 1/1 (Fig. 3, middle). Pure DOPC, as well as DOPC in the presence of mRNA, showed a negative zeta potential. As soon as DOTAP (without mRNA) was inserted into the membranes, the zeta potential was positive (see supplementary files for details). In the presence of both, DOTAP and mRNA, the zeta potential reflected the charge ratio of the components. In the case of an excess of DOTAP, the zeta potential was positive, while with an excess of mRNA, the zeta potential turned negative.

The insertion of the DOTAP and the mRNA into the membranes was further investigated by differential scanning calorimetry (DSC) measurements. In Fig. 4, results are shown as a function of DOTAP fraction, with and without mRNA. For the pure DOPC, a phase transition from the gel to the liquid-crystalline phase can be observed on the heating scans at subzero temperatures. For the systems prepared here, the phase transition was around -18 °C, where the phase transition temperature in the presence of mRNA was a bit higher than without. Insertion of DOTAP into the DOPC membranes induced a characteristic shift of the phase transition temperatures, first to lower, and then to higher values, where it monotonously increased as a function of the DOTAP fraction. For the effects of the DOTAP on the phase transition temperature of the DOPC, insertion in the gel and the liquid crystalline phase, as well as molecular interaction in both phases may contribute [32,33]. In the simplest case of a non-interacting solute which is only inserted into the liquid-crystalline (fluid-like) phase, a decrease of the phase transition temperature as a function of the solute concentration, according to

$$\Delta T_m = -\left(\frac{\mathrm{R}T_m^2}{\Delta H}\right) \cdot x_a$$

would be expected, where T_m is the phase transition temperature, ΔT_m is the shift of the phase transition temperature, R is the gas constant, ΔH is the melting enthalpy and x_a is the molar fraction of the solute in the solvent.

Here, such depression of the phase transition temperature occurs only at the lowest DOTAP fraction, and then the phase transition temperature increases. The increase is considered to be related to strong

electrostatic interactions between the positively charges DOTAP and the zwitterionic DOPC. More specifically, the attractive interactions between the positively charged trimethylammonium groups of the DOTAP and the negatively charged phosphate group of the DOPC are considered to provide the strongest contributions. However, further investigation will be necessary to unequivocally clarify these coherences. Importantly for the research questions in the current context, this general correlation of the phase transition temperature with the DOTAP fraction was maintained also in the presence of mRNA: the same decrease and increase of phase transition temperature with increasing DOTAP fraction was observed, where only minor shifts with respect to the mRNA-free samples occurred. Therefore, it is concluded that on the binding of the mRNA to the DOPC/DOTAP matrices, the mixed lipid system was maintained. No phase separation of the DOTAP out of the DOPC matrix, as induced by mRNA binding to DOTAP occurred, as this should have induced a shift of the phase transition temperature back to that of the pure DOPC system. In addition, the previously described observations on the zeta potential change with (+/-) ratio can be taken as an indication that both the mRNA and the DOTAP were in fact inserted into the membranes, as otherwise such effects on the zeta potential would not have been observed.

Cell culture experiments were performed, to test the principal functionality of the mRNA inserted into the lipid matrices. For this purpose, the concentrated lipid phases needed to be diluted before application to the cells. As a first test, the structure of the preparations was investigated upon dilution to check whether the molecular organization as found for the concentrated state was maintained. As an example, for three formulations with 90 mol% DOPC, 10 mol% DOTAP and 5, 10 or 20 mol% mRNA, dilution experiments were performed, and their structures were investigated with synchrotron radiation X-ray scattering measurements. Data for lipid concentrations of 100 mg/ml down to 0.5 mg/ml for this is shown in Fig. 5. As expected, peak intensity decreased with higher dilutions. However, the peak positions did not change, indicating the preservation of the molecular organization of the lipoplex system. Therefore, results from the structural characterization of the concentrated systems may be directly correlated with the outcome of the biological investigation.

Results from cell culture experiments using C2C12 murine myoblasts, shown in Fig. 6, demonstrate that the mRNA inserted in the lipid matrices was functional and luciferase expression depended on the characteristics of the respective systems. Higher signals were found with an excess of positive charge, however, also for the more negatively charged systems, the activity was proven. Further in vitro as well as in vivo, investigation of these systems will ensure the applicability of the system in different settings. Among these, local administration such as intradermal, intramuscular or intratumoral, where release over time may play a role, is considered promising. The most suitable type of composition may strongly depend on the therapeutic area and still needs to be identified.

DISCUSSION

Systems for mRNA delivery and release based on concentrated lamellar lipid phases were assembled and characterized with respect to their physicochemical characteristics and biological functionality. The results demonstrate that, by use of a low fraction of cationic lipid, mRNA can be inserted into zwitterionic lipid bilayer matrices in a controlled manner. Insertion was proven by SAXS and zeta potential measurements, as well as by measuring the residual free mRNA. The molecular organization of the formulations was maintained upon dilution, and the mRNA showed biological activity in cell culture experiments.

As illustrated in Fig. 7, a clear and concise model for the insertion of mRNA into DOPC/DOTAP-lipid bilayers was derived from the data. Structural changes were interpreted by observing the attractive and repulsive interactions between the components. DOTAP inserted homogeneously into the bilayer membranes as indicated by the shift of the phase transition temperature proportional to the DOTAP fraction. The tremendous increase of d-spacing and the loss of correlation between the bilayers

reflects the electrostatic repulsion in the presence of DOTAP in the bilayers. Accordingly, the zeta potential switched from negative to positive.

In the case of additionally present mRNA, the DOTAP acted as an anchor for inserting mRNA to the membranes, where a stoichiometric ratio between 1/1 and 2/1 for the DOTAP to mRNA ratio was maintained. The charge ratio (DOTAP to mRNA ratio) was decisive for the properties of the formulation. Two regimes, depending on the ratio between the positively charged DOTAP and the negatively charged mRNA were discerned: at an excess of the cationic lipid, mRNA integrated quantitatively into the membranes. In that regime, the lamellar organization was similar to that of pure, hydrated DOPC, indicating that the mRNA was accommodated in the membranes without exerting any additional electrostatic or steric effects on the d-spacing. Apparently, mRNA, together with other ionic moieties, was able to compensate the repulsive electrostatic interactions between the DOTAP in opposing bilayers even in the presence of excess DOTAP with respect to mRNA.

The observation that, given an excess of mRNA with respect to DOTAP in the membranes, the zeta potential became negative and the d-spacing increased monotonously with the mRNA excess indicates, that at least part of the excess mRNA is inserted between the bilayers beyond the fraction corresponding to that of the DOTAP. In all cases, the mRNA accounts only for a small fraction of the hydrophilic slab between the bilayers, as can be derived from the following conjectures:

The total d-spacing was about 70-80 Å for all systems comprising DOTAP and mRNA. As the d-spacing of dehydrated DOPC bilayers is estimated to be only about 40 Å, a water layer of about 20 Å in between the lipid bilayer is present. With the highest molar fraction of DOTAP tested here (10 mol%) and an estimated area per lipid of 75 $Å^2$, the hydrophilic volume per DOTAP amounts to

*75*10*40/2 $Å^3$= 15000 $Å^3$.*

(with 75 $Å^2$ for the area per lipid, 40 Å [34] the excess thickness of the hydrophilic slab, factor 10 as only 10 mol% DOTAP is in the bilayer and factor two because two bilayers share one hydrophilic slab).

The volume per nucleotide can be estimated as:

$330/1.5*10^{24}*/6*10^{23}$ = 367 $Å^3$/nucleotide

(With 330 Da as the molar mass per nucleotide and 1.5 g/mL the density of the mRNA, respectively)

which is about 2.5 % of the total available volume. Therefore in all cases, the mRNA in the bilayers is surrounded by a large excess of water, so that the mRNA might be oriented flat on the membranes, floating in an excess of water. For the effects on d-spacing of electrostatic interactions between all molecular moieties, including lipids, mRNA and counterions must be considered. For a clear answer towards how the mRNA is inserted into the bilayers and to model the different effects on d-spacing below and above charge equilibrium, further measurements like, for example, neutron scattering using contrast variation will be necessary. Such measurements are currently in preparation and will be presented in an upcoming publication.

In summary, in comparison to the much more extensively studied lipoplex systems comprising DNA [21–24], certain aspects of the mRNA lipid phases investigated here were similar. However, there are also distinct differences which may have to be considered for designing dedicated delivery systems for mRNA. Like many DNA lipoplexes, the mRNA phases were organized lamellar, where the mRNA was sandwiched in the hydrophobic slab in between adjacent lipid bilayers. Differences, and specific characteristics of the mRNA formulations, are revealed in the detailed internal organization of the mRNA in between the bilayers. mRNA, which is single stranded, has a much lower secondary order than the double stranded DNA which makes it more like a classical polyelectrolyte binding to a lipid bilayer membrane [35]. Here, in contrast to many earlier studies, only low fractions of mRNA were inserted into the hydrophilic slabs in a controlled manner. Insertion could be accurately fine-tuned by formulation parameters such as charge ratio and molar fraction of the cationic lipid in the membrane.

For DNA, over the years, extensive insight into the coherencies between molecular organization and formulation parameters like charge ratio could be achieved [36–39]. Further studies on the present systems comprising mRNA will be necessary to elucidate these correlations in comparison to the earlier studied systems. Such insight and ability for precise assembly of the delivery vehicles will be helpful for rational development of novel mRNA nanomedicines.

CONCLUSION

Messenger RNA was inserted into concentrated, lamellar phases from zwitterionic lipids using the cationic lipid DOTAP as an anchor. The molecular organization of the system and the kind of how the mRNA was inserted therein depended on the charge ratio, DOTAP to mRNA (nucleotide). The mRNA inserted into the aqueous slab between the lipid bilayer membranes and affected the d-spacing in an analytical manner. The RNA was released from the lipid matrices and displayed biological activity, as tested here by luciferase expression in cell culture models. Such obtained formulations may be promising as sustained release systems for various ways of local administration, like intradermal intramuscular or intratumoral injection.

ACKNOWLEDGEMENT

Funding by the “Deutsche Forschungsgemeinschaft” (SFB 1066) is gratefully acknowledged.

REFERENCES

(1) Kreiter, S.; Diken, M.; Selmi, A.; Türeci, Ö.; Sahin, U. Tumor Vaccination Using Messenger RNA: Prospects of a Future Therapy. *Curr. Opin. Immunol.* **2011**, *23* (3), 399–406.

(2) Türeci, Ö.; Vormehr, M.; Diken, M.; Kreiter, S.; Huber, C.; Sahin, U. Targeting the Heterogeneity of Cancer with Individualized Neoepitope Vaccines. *Clin. Cancer Res.* **2016**, *22* (8), 1885–1896.

(3) Kranz, L. M.; Diken, M.; Haas, H.; Kreiter, S.; Loquai, C.; Reuter, K. C.; Meng, M.; Fritz, D.; Vascotto, F.; Hefesha, H.; Grunwitz, C.; Vormehr, M.; Hüsemann, Y.; Selmi, A.; Kuhn, A. N.; Buck, J.; Derhovanessian, E.; Rae, R.; Attig, S.; Diekmann, J.; Jabulowsky, R. A.; Heesch, S.; Hassel, J.; Langguth, P.; Grabbe, S.; Huber, C.; Türeci, Ö.; Sahin, U. Systemic RNA Delivery to Dendritic Cells Exploits Antiviral Defence for Cancer Immunotherapy. *Nature* **2016**, *534* (7607), 396–401.

(4) Sahin, U.; Karikó, K.; Türeci, Ö. mRNA-Based Therapeutics--Developing a New Class of Drugs. *Nat. Rev. Drug Discov.* **2014**, *13* (10), 759–780.

(5) Grabbe, S.; Haas, H.; Diken, M.; Kranz, L. M.; Langguth, P.; Sahin, U. Translating Nanoparticulate-Personalized Cancer Vaccines into Clinical Applications: Case Study with RNA-Lipoplexes for the Treatment of Melanoma. *Nanomedicine (Lond).* **2016**, *11* (20), 2723–2734.

(6) Kreiter, S.; Vormehr, M.; van de Roemer, N.; Diken, M.; Löwer, M.; Diekmann, J.; Boegel, S.; Schrörs, B.; Vascotto, F.; Castle, J. C.; Tadmor, A. D.; Schoenberger, S. P.; Huber, C.; Türeci, Ö.; Sahin, U. Mutant MHC Class II Epitopes Drive Therapeutic Immune Responses to Cancer. *Nature* **2015**, *520* (7549), 692–696.

(7) Safinya, C. R.; Ewert, K. K.; Leal, C. Cationic Liposome–nucleic Acid Complexes: Liquid Crystal Phases with Applications in Gene Therapy. *Liq. Cryst.* **2011**, *38* (11–12), 1715–1723.

(8) Cullis, P. R.; Hope, M. J. Lipid Nanoparticle Systems for Enabling Gene Therapies. *Mol. Ther.* **2017**, *25* (7), 1467–1475.

(9) Xu, Y.; Hui, S. W.; Frederik, P.; Szoka, F. C. Physicochemical Characterization and Purification of Cationic Lipoplexes. *Biophys. J.* **1999**, *77* (July), 341–353.

(10) Rice, J.; Ottensmeier, C. H.; Stevenson, F. K. DNA Vaccines: Precision Tools for Activating Effective Immunity against Cancer. *Nat. Rev. Cancer* **2008**, *8* (2), 108–120.

(11) Malone, R. W.; Felgner, P. L.; Verma, I. M. Cationic Liposome-Mediated RNA Transfection. *Proc. Natl. Acad. Sci. U. S. A.* **1989**, *86* (16), 6077–6081.

(12) Boczkowski, D.; Nair, S. K.; Snyder, D.; Gilboa, E. Dendritic Cells Pulsed with RNA Are Potent Antigen-Presenting Cells in Vitro and in Vivo. *J. Exp. Med.* **1996**, *184* (2), 465–472.

(13) Bringmann, A.; Held, S. A. E.; Heine, A.; Brossart, P. RNA Vaccines in Cancer Treatment. *J. Biomed. Biotechnol.* **2010**, *2010*, 623687.

(14) Kallen, K.-J.; Theß, A. A Development That May Evolve into a Revolution in Medicine: mRNA as the Basis for Novel, Nucleotide-Based Vaccines and Drugs. *Ther. Adv. vaccines* **2014**, *2* (1), 10–31.

(15) Ma, B.; Zhang, S.; Jiang, H.; Zhao, B.; Lv, H. Lipoplex Morphologies and Their Influences on Transfection Efficiency in Gene Delivery. *J. Control. Release* **2007**, *123* (3), 184–194.

(16) Khatri, N.; Baradia, D.; Vhora, I.; Rathi, M.; Misra, A. cRGD Grafted Liposomes Containing Inorganic Nano-Precipitate Complexed siRNA for Intracellular Delivery in Cancer Cells. *J.*

Control. Release **2014**, *182*, 45–57.

(17) Dan, N.; Danino, D. Structure and Kinetics of Lipid-Nucleic Acid Complexes. *Adv. Colloid Interface Sci.* **2014**, *205*, 230–239.

(18) Hirko, A.; Tang, F.; Hughes, J. Cationic Lipid Vectors for Plasmid DNA Delivery. *Curr. Med. Chem.* **2003**, *10* (14), 1185–1193.

(19) Semple, S. C.; Akinc, A.; Chen, J.; Sandhu, A. P.; Mui, B. L.; Cho, C. K.; Sah, D. W. Y.; Stebbing, D.; Crosley, E. J.; Yaworski, E.; Hafez, I. M.; Dorkin, J. R.; Qin, J.; Lam, K.; Rajeev, K. G.; Wong, K. F.; Jeffs, L. B.; Nechev, L.; Eisenhardt, M. L.; Jayaraman, M.; Kazem, M.; Maier, M. A.; Srinivasulu, M.; Weinstein, M. J.; Chen, Q.; Alvarez, R.; Barros, S. A.; De, S.; Klimuk, S. K.; Borland, T.; Kosovrasti, V.; Cantley, W. L.; Tam, Y. K.; Manoharan, M.; Ciufolini, M. A.; Tracy, M. A.; de Fougerolles, A.; MacLachlan, I.; Cullis, P. R.; Madden, T. D.; Hope, M. J. Rational Design of Cationic Lipids for siRNA Delivery. *Nat. Biotechnol.* **2010**, *28* (2), 172–176.

(20) Janich, C.; Taßler, S.; Meister, A.; Hause, G.; Schäfer, J.; Bakowsky, U.; Brezesinski, G.; Wölk, C. Structures of Malonic Acid Diamide/phospholipid Composites and Their Lipoplexes. *Soft Matter* **2016**, *12* (27), 5854–5866.

(21) Rädler, J. O.; Koltover, I.; Salditt, T.; Safinya, C. R. Structure of DNA-Cationic Liposome Complexes: DNA Intercalation in Multilamellar Membranes in Distinct Interhelical Packing Regimes. *Science* **1997**, *275* (5301), 810–814.

(22) Koltover, I.; Salditt, T.; Safinya, C. R. Phase Diagram, Stability, and Overcharging of Lamellar Cationic Lipid-DNA Self-Assembled Complexes. *Biophys. J.* **1999**, *77* (2), 915–924.

(23) Majzoub, R. N.; Ewert, K. K.; Safinya, C. R. Cationic Liposome-Nucleic Acid Nanoparticle Assemblies with Applications in Gene Delivery and Gene Silencing. *Philos. Trans. A. Math. Phys. Eng. Sci.* **2016**, *374* (2072), 20150129.

(24) Salditt, T.; Koltover, I.; Rädler, J. O.; Safinya, C. R. Two-Dimensional Smectic Ordering of Linear DNA Chains in Self-Assembled DNA-Cationic Liposome Mixtures. *Phys. Rev. Lett.* **1997**, *79* (13), 2582–2585.

(25) Di Cola, E.; Grillo, I.; Ristori, S. Small Angle X-Ray and Neutron Scattering: Powerful Tools for Studying the Structure of Drug-Loaded Liposomes. *Pharmaceutics* **2016**, *8* (2), 1–16.

(26) Wu, P.; Yu, Y.; McGhee, C. E.; Tan, L. H.; Lu, Y. Applications of Synchrotron-Based Spectroscopic Techniques in Studying Nucleic Acids and Nucleic Acid-Functionalized Nanomaterials. *Adv. Mater.* **2014**, *26* (46), 7849–7872.

(27) Pollard, C.; Rejman, J.; De Haes, W.; Verrier, B.; Van Gulck, E.; Naessens, T.; De Smedt, S.; Bogaert, P.; Grooten, J.; Vanham, G.; De Koker, S. Type I IFN Counteracts the Induction of Antigen-Specific Immune Responses by Lipid-Based Delivery of mRNA Vaccines. *Mol. Ther.* **2013**, *21* (1), 251–259.

(28) Simberg, D.; Weisman, S.; Talmon, Y.; Barenholz, Y. DOTAP (and Other Cationic Lipids): Chemistry, Biophysics, and Transfection. *Crit. Rev. Ther. Drug Carrier Syst.* **2004**, *21* (4), 257–317.

(29) Lee, E. R.; Marshall, J.; Siegel, C. S.; Jiang, C.; Yew, N. S.; Nichols, M. R.; Nietupski, J. B.; Ziegler, R. J.; Lane, M. B.; Wang, K. X.; Wan, N. C.; Scheule, R. K.; Harris, D. J.; Smith, A. E.; Cheng, S. H. Detailed Analysis of Structures and Formulations of Cationic Lipids for Efficient Gene Transfer to the Lung. *Hum. Gene Ther.* **1996**, *7* (14), 1701–1717.

(30) Kuhn, A. N.; Diken, M.; Kreiter, S.; Selmi, A.; Kowalska, J.; Jemielity, J.; Darzynkiewicz, E.; Huber, C.; Türeci, Ö.; Sahin, U. Phosphorothioate Cap Analogs Increase Stability and

Translational Efficiency of RNA Vaccines in Immature Dendritic Cells and Induce Superior Immune Responses in Vivo. *Gene Ther.* **2010**, *17* (8), 961–971.

(31) Crowe, L. M.; Reid, D. S.; Crowe, J. H. Is Trehalose Special for Preserving Dry Biomaterials? *Biophys. J.* **1996**, *71* (4), 2087–2093.

(32) Jain, M. K.; Wu, N. M. Effect of Small Molecules on the Dipalmitoyl Lecithin Liposomal Bilayer: III. Phase Transition in Lipid Bilayer. *J. Membr. Biol.* **1977**, *34* (1), 157–201.

(33) Lohner, K. Effects of Small Organic Molecules on Phospholidpid Phase Transitions. *Chem. Phys. Lipids* **1991**, *57* (2–3), 341–362.

(34) Cavalcanti, L. P.; Konovalov, O.; Haas, H. X-Ray Diffraction from Paclitaxel-Loaded Zwitterionic and Cationic Model Membranes. *Chem. Phys. Lipids* **2007**, *150* (1), 58–65.

(35) Yang, L.; Liang, H.; Angelini, T. E.; Butler, J.; Coridan, R.; Tang, J. X.; Wong, G. C. L. Self-Assembled Virus–membrane Complexes. *Nat. Mater.* **2004**, *3* (9), 615–619.

(36) Bruinsma, R. Electrostatics of DNA-Cationic Lipid Complexes: Isoelectric Instability. *Eur. Phys. J. B* **1998**, *4* (1), 75–88.

(37) Bruinsma, R.; Mashl, J. Long-Range Electrostatic Interaction in DNA-Cationic Lipid Complexes. *Europhys. Lett.* **1998**, *41* (2), 165–170.

(38) Golubović, L.; Golubović, M. Fluctuations of Quasi-Two-Dimensional Smectics Intercalated between Membranes in Multilamellar Phases of DNA-Cationic Lipid Complexes. *Phys. Rev. Lett.* **1998**, *80* (19), 4341–4344.

(39) O'Hern, C. S.; Lubensky, T. C. Sliding Columnar Phase of DNA-Lipid Complexes. **1997**.

FIGURE CAPTIONS

Fig. 0: Cover

Fig. 1: Scattering curves (SAXS) from lipoplexes with EPC, DOTAP and mRNA with a lipid concentration of 100 mg/ml, measured in 10 % trehalose. Data show pure EPC [black], EPC in presence of 5% mRNA [red], EPC and 5 mol% DOTAP [green], EPC and 5 mol% DOTAP in the presence of 5 mol% mRNA (+/- = 1/1) [blue], EPC and 5 mol% DOTAP in the presence of 10 mol% mRNA (+/- = $1/2$) [cyan].

Fig. 2: Scattering curves (SAXS) from lipoplexes with DOPC, DOTAP and mRNA with a lipid concentration of 100 mg/ml, measured in 10 % trehalose. Data show pure DOPC [black], DOPC and 5 mol% DOTAP [red], DOPC and 5 mol% of DOTAP in the presence of 2.5 mol% mRNA (+/- = 2/1) [green], DOPC with 5 mol% of DOTAP in the presence of 5 mol% of mRNA (+/- = 1/1) [blue], DOPC with 5 mol% of DOTAP in the presence of 10 mol% mRNA (+/- = $1/2$) [cyan], DOPC with 5 mol% of DOTAP in the presence of 20 mol% mRNA (+/- = $1/4$) [purple].

Fig. 3: Analytical characterization of lipoplexes showing a., d-spacing of lipoplexes with different proportions of DOPC, DOTAP and mRNA, b., zeta potential of lipoplexes with different amounts of DOPC, DOTAP and 20 mol% mRNA and c., amount of free mRNA from DOPC with different amounts of DOTAP and 20 mol% mRNA; plotted as a function of the DOTAP to mRNA (+/-) ratio.

Fig. 4: Phase transition temperature of lipoplexes with different proportions of DOPC, DOTAP and mRNA; plotted as a function of the amount of DOTAP.

Fig. 5: Scattering curves (SAXS) from DOPC with 10 mol% DOTAP and a. 5 mol% mRNA, b. 10 mol% mRNA and c. 20 mol% mRNA, diluted up to a lipid concentration of 0.5 mg/ml.

Fig. 6: Transfection in C2C12 cells and cell viability of lipoplexes with DOPC, different amounts of DOTAP and 20 mol% mRNA.

Fig. 7: Lattice model (top view) o lipid layers illustrating the organization of mRNA at the lipid layer (top) and side view of a lipid bilayer illustrating the insertion of a DOTAP molecule and a nucleotide into the lipid membrane (bottom)

SUPPORTING INFORMATION

Fig. 8: Scattering curves (SAXS) from lipoplexes with DOPC, DOTAP and mRNA with a lipid concentration of 100 mg/ml, measured in 10 % trehalose. Data show pure DOPC [black], DOPC and 2.5 mol% DOTAP [red], DOPC and 2.5 mol% of DOTAP in the presence of 2.5 mol% mRNA (+/- = 1/1) [green], DOPC with 2.5 mol% of DOTAP in the presence of 5 mol% of RNA (+/- = 1/2) [blue], DOPC with 2.5 mol% of DOTAP in the presence of 10 mol% mRNA (+/- = $1/4$) [cyan], DOPC with 2.5 mol% of DOTAP in the presence of 20 mol% mRNA (+/- = $1/8$) [purple].

Fig. 9: Scattering curves (SAXS) from lipoplexes with DOPC, DOTAP and mRNA with a lipid concentration of 100 mg/ml, measured in 10 % trehalose. Data show pure DOPC [black], DOPC and 10 mol% DOTAP [red], DOPC and 10 mol% of DOTAP in the presence of 2.5 mol% mRNA (+/- = 4/1) [green], DOPC with 10 mol% of DOTAP in the presence of 5 mol% of RNA (+/- = 2/1) [blue], DOPC with 10 mol% of DOTAP in the presence of 10 mol% mRNA (+/- = $1/1$) [cyan], DOPC with 10 mol% of DOTAP in the presence of 20 mol% mRNA (+/- = $1/2$) [purple].

Table 3: Data for d-spacing of lipoplexes with different proportions of DOPC, DOTAP and mRNA; shown in Fig. 3

Table 4: Data for zeta potential and amount of free mRNA of lipoplexes with different amounts of DOPC, DOTAP and 20 mol% mRNA; shown in Fig. 3.

Table 5: Data for phase transition temperature of lipoplexes with different proportions of DOPC, DOTAP and mRNA shown in Fig. 4.

Table 6: Data for transfection and cell viability of lipoplexes with DOPC, different amounts of DOTAP and 20 mol% mRNA; shown in Fig. 6.

Table 7: Calculated volume fraction of the mRNA in the aqueous slab for different amounts of DOTAP.

FIGURES

Fig. 0: Graphical abstract

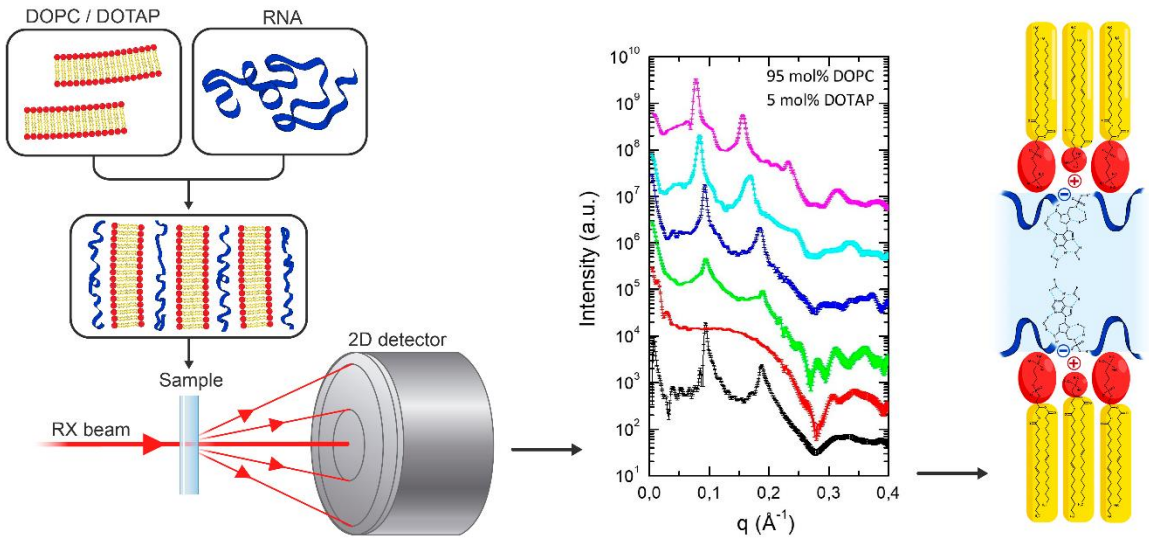

Fig. 1:

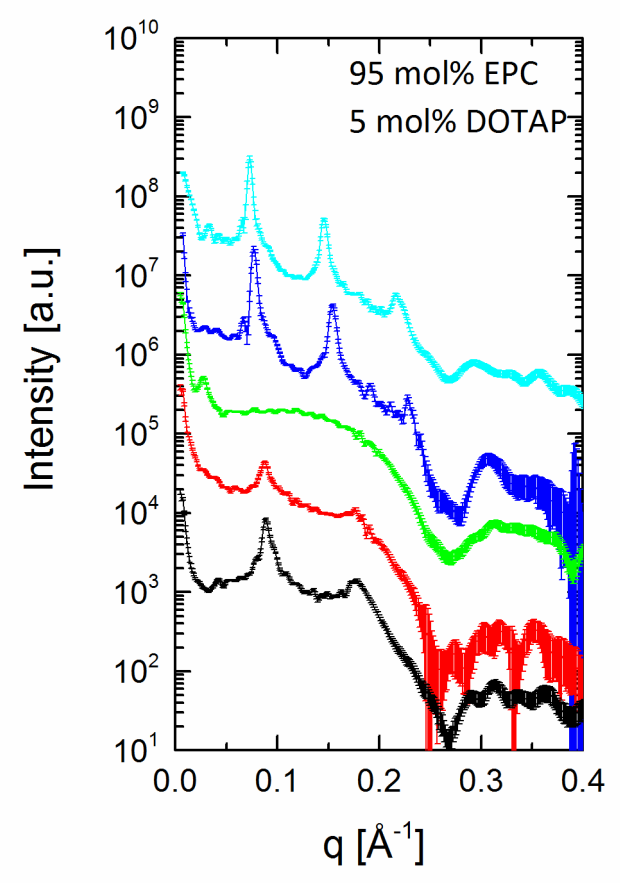
95 mol% EPC
5 mol% DOTAP
Intensity [a.u.]
q [Å^{-1}]
10^{10}
10^{9}
10^{8}
10^{7}
10^{6}
10^{5}
10^{4}
10^{3}
10^{2}
10^{1}
0.0
0.1
0.2
0.3
0.4

640 Fig. 2:

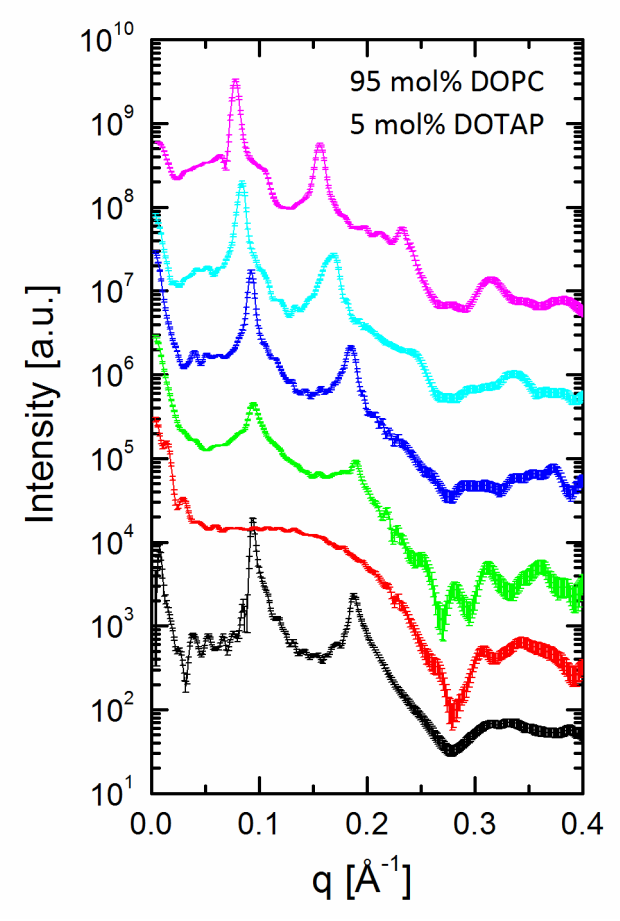

641

642

643

644

645

646

647

Fig. 3:

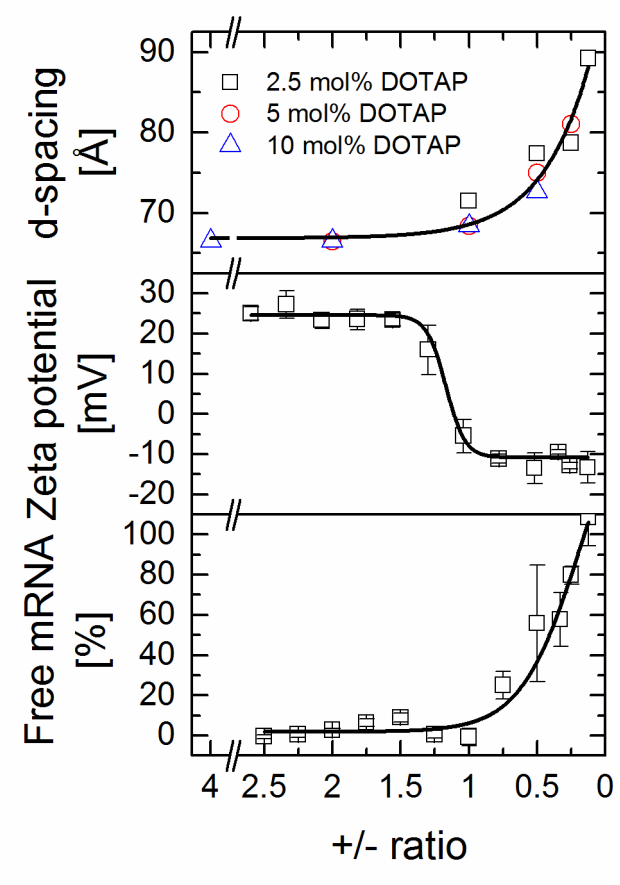
d-spacing [Å]
Zeta potential [mV]
Free mRNA [%]
2.5 mol% DOTAP
5 mol% DOTAP
10 mol% DOTAP
+/- ratio

666 Fig. 4:

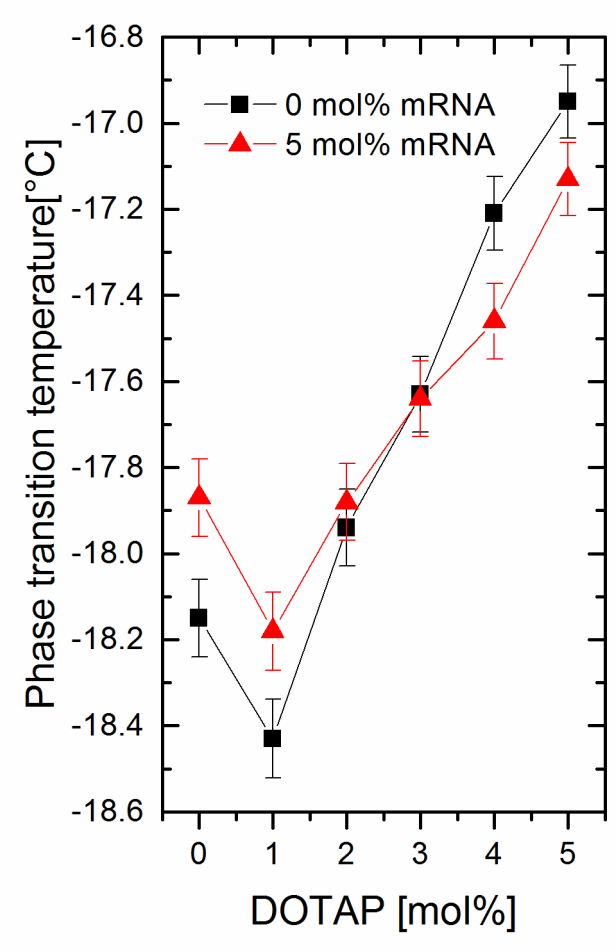

667

668

669 Fig. 5:

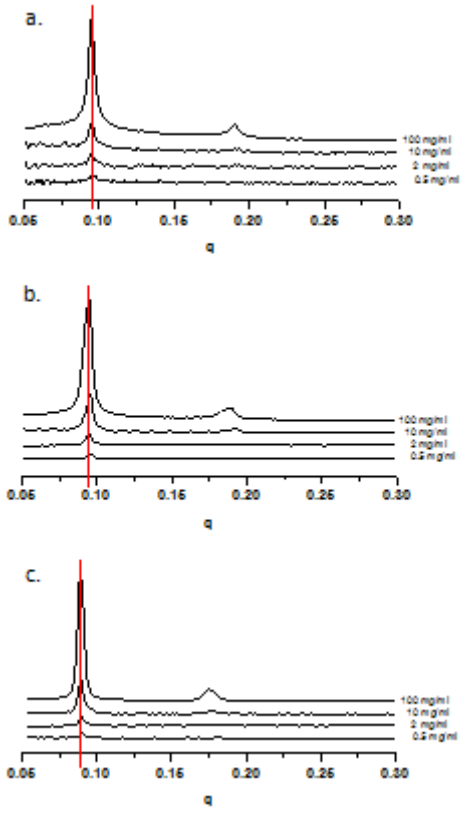

670

671

672

673

674

675

676

677

678

679

680

681

682 Fig. 6:

683

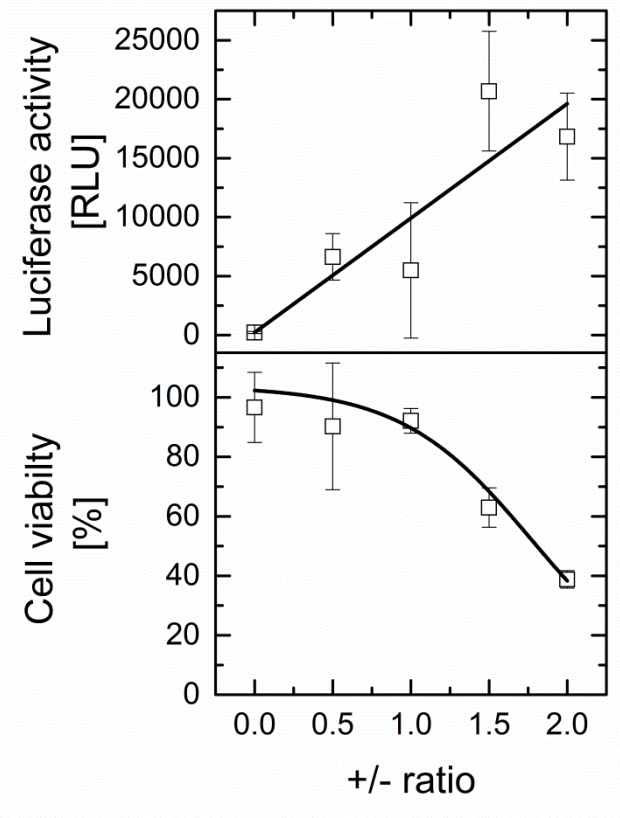

684

685

686

687 Fig. 7:

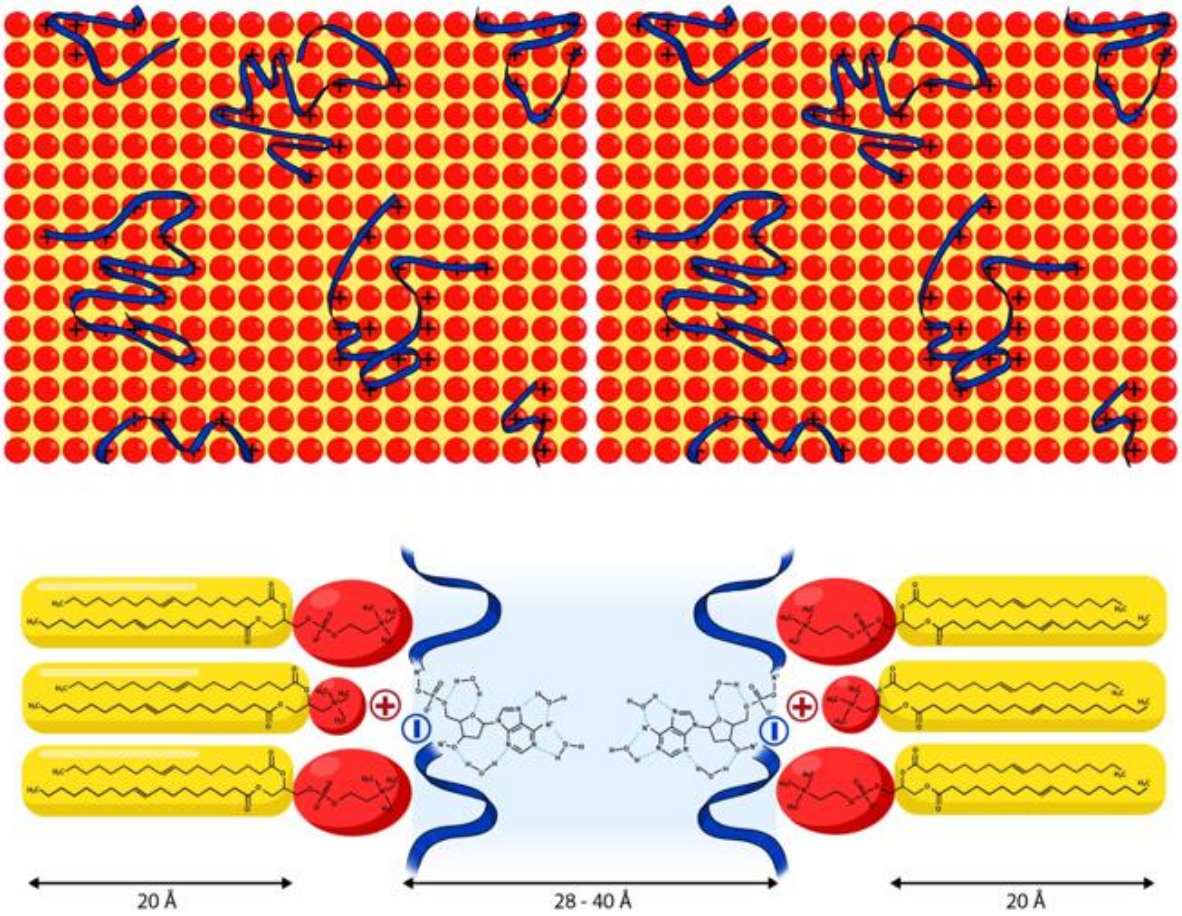

688

689

690